

Novel Virtual Simply Supported Beam Method for Detecting the Speed and Axles of Moving Vehicles on Bridges

Wei He¹; Lu Deng, Ph.D., M.ASCE²; Hai Shi³; C. S. Cai, F.ASCE⁴; and Yang Yu⁵

Abstract: One of the major drawbacks with most bridge weigh-in-motion (BWIM) methods that adopt the Moses algorithm is the need for acquisition of vehicle speed and axle spacing by using additional devices, such as free-of-axle detectors. This study presents a novel virtual simply supported beam (VSSB) method, which uses weighing sensors to directly identify the speed and the axle spacing of passing vehicles on bridges, making it very desirable for commercial BWIM systems. Numerical simulations and model tests are carried out to study the effectiveness and accuracy of the proposed method. The results show that the proposed method can successfully identify the vehicle speed and axle spacing with good accuracy. The proposed method also proves reliable under noisy conditions. **DOI:** [10.1061/\(ASCE\)BE.1943-5592.0001019](https://doi.org/10.1061/(ASCE)BE.1943-5592.0001019). © 2016 American Society of Civil Engineers.

Author keywords: Virtual simply supported beam method; Bridge weigh-in-motion; Strain; Speed; Axle spacing; Vehicle weight.

Introduction

Accurate and reliable traffic information, including both the gross weight and axle weights of passing vehicles, is very important not only for the design of bridges and pavements but also for their monitoring and retrofitting (Fryba 1999; Wu and Chen 2009; Zhu and Law 2000). Recently, researchers proposed different methods for identifying the parameters of vehicles. For example, Law et al. (1997) proposed a moving force identification (MFI) method to identify vehicle loads; Feng et al. (2015) proposed a method that can simultaneously identify the parameters of the bridge and the vehicle loads. The recently developed bridge weigh-in-motion (BWIM) technique provides a convenient and cost-effective method to predict the axle loads of vehicles indirectly using instrumented bridges. The basic concept was first introduced by Moses in the 1970s (Moses 1979). In the past several decades, extensive research has been devoted to the development of new BWIM models and the improvement of the accuracy of BWIM systems (Jacob and O'Brien 1998; O'Brien et al. 1999; Peters 1984; WAVE 2001). A comprehensive review of the recent developments in the BWIM technique is available in Lydon et al. (2015).

Accurate identification of vehicle speed and axle spacing is a prerequisite for most BWIM systems to correctly identify the axle weights and gross weight of vehicles. A typical BWIM system

consists of two main components, one for detecting the vehicle axles, and the other for measuring bridge responses (usually strains) to achieve the purpose of weight identification (Moses 1979). Traditional instruments for axle detection include tape switches and pneumatic tubes, which are quite simple to install and have shown satisfactory accuracy. However, they are not durable and will cause disruption to traffic during installation and replacement. Recently, the concept of a nothing-on-road (NOR) system was proposed with the goal of freeing the use of axle detectors on the road surface. The free-of-axle detector (FAD) algorithm, which is one application of the NOR BWIM systems, was first proposed in the Weighing-in-Motion of Axles and Vehicles for Europe (WAVE) project (WAVE 2001). However, the applicability of the FAD algorithm is still limited due to the restrictions it poses on the bridge span length, superstructure thickness, and deck surface condition (Kalin et al. 2006; WAVE 2001). In addition, it still requires installation of additional FAD sensors.

In addition to using flexural strains to detect vehicle axles, some researchers also recently proposed the use of other bridge responses for axle detection. O'Brien et al. (2012) proposed the use of shear strains to detect axle information. Bao et al. (2016) also used shear strains to identify axles as well as vehicle weights. Feng and Feng (2015) identified vehicle speed by minimizing the error between the measured and predicted bridge displacement time histories.

For flexural strain-based BWIM systems, it is very desirable to directly utilize the global flexural strain information obtained from the weighing sensors to identify the vehicle speed and axle spacing. Nonetheless, achieving axle identification from the global strain signal is very difficult because the signal does not usually have a sharp peak upon the passage of each axle. Recently, wavelet transformation has proven to be a potential technique for axle detection by some researchers (Chatterjee et al. 2006; Dunne et al. 2005), although more research is still needed to improve the reliability of this technique, especially under circumstances in which errors exist in the original raw data and can be magnified in the wavelet analysis results (Lydon et al. 2015).

In this paper, a novel virtual simply supported beam (VSSB) method was proposed to identify the vehicle speed and the axle spacing by using the flexural strain signal obtained from the weighing sensors. Compared to other NOR systems, the proposed method does not require additional sensors of other types for detecting

¹Research Assistant, College of Civil Engineering, Hunan Univ., Changsha, Hunan 410082, China. E-mail: hewei.hnu@gmail.com

²Professor, Key Laboratory for Wind and Bridge Engineering of Hunan Province, Hunan Univ., Changsha, Hunan 410082, China (corresponding author). E-mail: denglu@hnu.edu.cn

³Research Assistant, College of Civil Engineering, Hunan Univ., Changsha, Hunan 410082, China. E-mail: shihai0720@qq.com

⁴Professor, Dept. of Civil and Environmental Engineering, Louisiana State Univ., Baton Rouge, LA 70803. E-mail: cscai@lsu.edu

⁵Research Assistant, Dept. of Civil and Environmental Engineering, Louisiana State Univ., Baton Rouge, LA 70803. E-mail: josephyangyu@gmail.com

Note. This manuscript was submitted on August 10, 2016; approved on October 13, 2016; published online on December 7, 2016. Discussion period open until May 7, 2017; separate discussions must be submitted for individual papers. This paper is part of the *Journal of Bridge Engineering*, © ASCE, ISSN 1084-0702.

vehicle speed and axles. The effectiveness and accuracy of the proposed method were demonstrated through numerical simulations based on a three-dimensional vehicle–bridge coupled system. A simply supported multigirder concrete bridge and three different types of trucks were adopted in the numerical simulation for illustration. The effects of various factors on the accuracy of the proposed method were investigated.

Vehicle–Bridge Coupled System

Equation of Motion of Vehicle

Based on the theory of structural dynamics, the equation of motion can be written as follows for a vehicle:

$$[\mathbf{M}_v]\{\ddot{\mathbf{d}}_v\} + [\mathbf{C}_v]\{\dot{\mathbf{d}}_v\} + [\mathbf{K}_v]\{\mathbf{d}_v\} = \{\mathbf{F}_G\} + \{\mathbf{F}_v\} \quad (1)$$

where $[\mathbf{M}_v]$, $[\mathbf{C}_v]$, and $[\mathbf{K}_v]$ = vehicle mass, damping, and stiffness matrices, respectively; $\{\mathbf{d}_v\}$ = vehicle displacement vector in the vertical direction; $\{\mathbf{F}_G\}$ = gravity force vector of the vehicle; and $\{\mathbf{F}_v\}$ = vector of the wheel–road contact forces acting on the vehicle.

Equation of Motion of Bridge

Similarly, the equation of motion for a bridge can be written as follows:

$$[\mathbf{M}_b]\{\ddot{\mathbf{d}}_b\} + [\mathbf{C}_b]\{\dot{\mathbf{d}}_b\} + [\mathbf{K}_b]\{\mathbf{d}_b\} = \{\mathbf{F}_b\} \quad (2)$$

where $[\mathbf{M}_b]$, $[\mathbf{C}_b]$, and $[\mathbf{K}_b]$ = mass, damping, and stiffness matrices of the bridge, respectively; $\{\mathbf{d}_b\}$ = bridge displacement vector; and $\{\mathbf{F}_b\}$ = vector of the wheel–road contact forces acting on the bridge, which is actually the reaction force vector to $\{\mathbf{F}_v\}$.

Road Surface Condition

The road surface roughness is an important source of excitation for the vibration of the vehicle–bridge system. A road surface profile can be assumed to be a zero-mean stationary Gaussian random process and can be generated through an inverse Fourier transformation based on a power spectral density (PSD) function (Dodds and Robson 1973). In this study, the following expression was used for generating the road surface profile:

$$r(x) = \sum_{k=1}^N \sqrt{2\varphi(n_k)\Delta n} \cos(2\pi n_k x + \theta_k) \quad (3)$$

where θ_k = random phase angle, which has a uniform distribution within $0-2\pi$; $\varphi()$ = PSD function for the road surface elevation ($\text{m}^3/\text{cycle}/\text{m}$); and n_k = wave number (cycle/m). In the present study, a modified PSD function (Huang and Wang 1992) was adopted

$$\varphi(n) = \varphi(n_0) \left(\frac{n}{n_0}\right)^{-2} \quad (n_1 < n < n_2) \quad (4)$$

where n = spatial frequency (cycle/m); n_0 = discontinuity frequency of 0.5π (cycle/m); $\varphi(n_0)$ = roughness coefficient (m^3/cycle); and n_1 and n_2 = lower and upper cutoff frequencies, respectively. The International Organization for Standardization (ISO 1995) classified the road surface condition (RSC) based on different roughness

coefficients. Based on the ISO classification, a total of four different road surface conditions (smooth, very good, good, and average) were considered in the present study, with corresponding roughness coefficients of 0 , 5×10^{-6} , 20×10^{-6} , and 80×10^{-6} m^3/cycle , respectively.

Assembling Vehicle–Bridge Coupled System

By utilizing the displacement relationship and the interaction force relationship at the wheel–road contact points, the vehicle–bridge coupled system can be established by combining the equations of motion of both the bridge and the vehicle (Deng and Cai 2010), as follows:

$$\begin{bmatrix} \mathbf{M}_b & \\ & \mathbf{M}_v \end{bmatrix} \begin{Bmatrix} \ddot{\mathbf{d}}_b \\ \ddot{\mathbf{d}}_v \end{Bmatrix} + \begin{bmatrix} \mathbf{C}_b + \mathbf{C}_{b-b} & \mathbf{C}_{b-v} \\ \mathbf{C}_{v-b} & \mathbf{C}_v \end{bmatrix} \begin{Bmatrix} \dot{\mathbf{d}}_b \\ \dot{\mathbf{d}}_v \end{Bmatrix} + \begin{bmatrix} \mathbf{K}_b + \mathbf{K}_{b-b} & \mathbf{K}_{b-v} \\ \mathbf{K}_{v-b} & \mathbf{K}_v \end{bmatrix} \begin{Bmatrix} \mathbf{d}_b \\ \mathbf{d}_v \end{Bmatrix} = \begin{Bmatrix} \mathbf{F}_{b-r} \\ \mathbf{F}_G + \mathbf{F}_{v-r} \end{Bmatrix} \quad (5)$$

where \mathbf{C}_{b-b} , \mathbf{C}_{b-v} , \mathbf{C}_{v-b} , \mathbf{K}_{b-b} , \mathbf{K}_{b-v} , \mathbf{K}_{v-b} , \mathbf{F}_{b-r} , and \mathbf{F}_{v-r} = time-dependent terms related to the wheel–road contact forces. The dynamic Eq. (5) can be solved using the fourth-order Runge-Kutta method. A computer program was developed using MATLAB to assemble the matrices into Eq. (5), which was then solved by using the Newmark- β method in the time domain. More details about the vehicle–bridge coupled system and how road roughness affects the vehicle–bridge coupled vibration can be found in Deng and Cai (2010). The developed bridge–vehicle coupled model has also been validated using field measurements by Cai et al. (2007) and Deng and Cai (2011).

After obtaining the bridge dynamic responses, the stress of the bridge can be obtained by

$$[\mathbf{S}] = [\mathbf{E}][\mathbf{B}]\{\mathbf{d}_b\} \quad (6)$$

where $[\mathbf{E}]$ = stress-strain relationship matrix and can be assumed as constant over the same element; and $[\mathbf{B}]$ = strain-displacement relationship matrix assembled with the derivatives of the element shape functions with respect to x , y , and z , which are derived following a standard finite-element formulation process.

Methodology for Detecting Vehicle Speed and Axles

VSSB Method

Fig. 1(a) shows a linear-elastic Beam AB with arbitrary boundary conditions. Points O , P , and Q are three consecutive points on the beam. The distances between the adjacent points are marked. The beam is subjected to a concentrated force (F) at a distance of x from Point P . The end forces (including shear force and bending moment) applied at the two ends of Beam AB, which can be reaction forces if Points A and B are the end supports or internal forces if Beam AB is a segment of a beam, are assumed to be F_A , F_B , M_A , and M_B .

Based on the superposition principle, the bending moment of Beam AB at Locations O , P , and Q can be expressed as follows:

$$M_s = M_s^E + M_s^F, \quad s = \{O, P, Q\} \quad (7)$$

where M_s^E = moment of Beam AB caused by the end forces; and M_s^F = moment of Beam AB caused by the concentrated force (F).

Apparently, from Fig. 1(a), the following relationships hold:

$$\begin{aligned} M_O^E &= M_A + F_A(l_A + l) \\ M_P^E &= M_A + F_A l_A \\ M_Q^E &= M_A + F_A(l_A + 2l) \end{aligned} \quad (8)$$

The bending moment (M_s^F) caused by the concentrated force (F) can be calculated by using the following equations:

$$\begin{aligned} M_O^F &= \begin{cases} F(x-l) & x < l \\ 0 & x \geq l \end{cases} \\ M_P^F &= \begin{cases} Fx & x < 0 \\ 0 & x \geq 0 \end{cases} \\ M_Q^F &= \begin{cases} F(x-2l) & x < 2l \\ 0 & x \geq 2l \end{cases} \end{aligned} \quad (9)$$

From Eqs. (7)–(9), it is not difficult to determine that

$$M_O^E - \frac{1}{2}(M_P^E + M_Q^E) = 0 \quad (10)$$

and

$$M_O - \frac{1}{2}(M_P + M_Q) = \begin{cases} 0 & (x < 0 \text{ or } x \geq 2l) \\ \frac{1}{2}Fx & (0 \leq x < l) \\ \frac{1}{2}F(2l-x) & (l \leq x < 2l) \end{cases} \quad (11)$$

where M_O , M_P , and M_Q = bending moments at the three Points O , P , and Q , respectively. For the convenience of discussion, M_O^I is defined as follows:

$$M_O^I = M_O - \frac{1}{2}(M_P + M_Q) \quad (12)$$

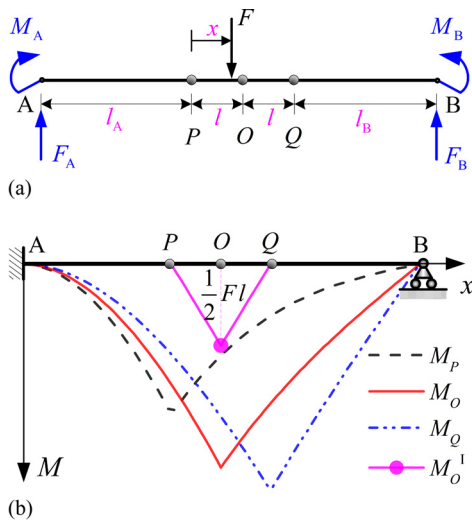


Fig. 1. Schematic of VSSB method: (a) Beam AB with arbitrary boundary conditions; (b) illustration of VSSB

Eqs. (11) and (12) show that M_O^I is only related to the distances between the force (F) and the three Points O , P , and Q , whereas it has nothing to do with the boundary condition of Beam AB. In fact, M_O^I is equal to the moment at Point O on the Beam Segment PQ , assuming that Segment PQ is simply supported at both ends and is only subjected to the concentrated force (F). Because M_O^I is independent of the boundary condition of the isolated Segment PQ , it is called the *isolated moment of Point O*, and the isolated Beam Segment PQ (which contains Point O) is referred to as the VSSB hereafter in this paper.

Although the lengths of OP and OQ were set to equal when introducing the theory of the proposed VSSB method, the proposed method does not actually require equal length for these two segments (OP and OQ). If OP and OQ have different lengths, the isolated moment (M_O^I) can be easily calculated as follows:

$$M_O^I = M_O - \frac{1}{l_{OP} + l_{OQ}}(l_{OQ}M_P + l_{OP}M_Q) \quad (13)$$

where l_{OP} and l_{OQ} = length of OP and length of OQ , respectively. To illustrate the proposed concept and its applicability, Fig. 1(b) shows a beam that is fixed at the left end and supported by a roller on the right. As a matter of fact, the proposed method does not set any requirement on the boundary conditions, as discussed previously. The influence lines of the bending moments of O , P , and Q and the moment M_O^I of Point O on the VSSB PQ under a moving force are also plotted in Fig. 1(b). From Fig. 1(b), it is very clear that each of the four influence lines has an obvious valley when the force moves across Beam AB.

Axle Detection

To identify the axles of passing vehicles, two groups of points ($\{P_1, O_1, Q_1\}$ and $\{P_2, O_2, Q_2\}$) were first picked. The distance between the adjacent points within the same group is set to l . The distance between the two groups of points is L , as shown in Fig. 2. Then, based on the calculation of M_O^I as shown in Eq. (12), the isolated bending moment at Points O_1 and O_2 on the two VSSB (P_1Q_1 and P_2Q_2 ; i.e., $M_{O_1}^I$ and $M_{O_2}^I$) can be obtained in a similar fashion. Fig. 1(b) shows that, when a force moves across the beam, a valley appears in the influence line. As a result, when N concentrated forces move across the beam, N turning points appear on the curves of the isolated moments $M_{O_1}^I$ and $M_{O_2}^I$.

For illustration, Fig. 3 plots the bending moments and the isolated moments under two moving loads with a distance of d . First, as can be seen from Fig. 3, the number of valleys on the isolated moments ($M_{O_1}^I$ and $M_{O_2}^I$) is equal to the number of moving loads. Second, the valleys on the curve of $M_{O_1}^I$ occur (at Times t_1^1 and t_2^1) earlier than those on $M_{O_2}^I$ (at Times t_1^2 and t_2^2) by ΔT , assuming that the loads move from left to right. Therefore, the velocity of the moving loads can be easily predicted by the following equation:

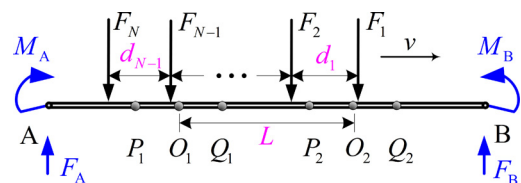


Fig. 2. Two VSSBs for axle detection

$$v = \frac{L}{\Delta T} = \frac{L}{t_1^2 - t_1^1} \quad \text{or} \quad v = \frac{L}{t_2^2 - t_2^1} \quad (14)$$

An alternative algorithm proposed by Kalin et al. (2006) can also be used to determine the vehicle speed. This method calculates the cross correlation of two discrete-time sequences (for instance, $M_{O_1}^1$ and $M_{O_2}^1$ in the present study) to find their time lag, and has proven to provide robust results.

It is also observed that there are time gaps between the adjacent valleys on the isolated moment curves. For example, the two valleys on the curve of $M_{O_2}^1$ in Fig. 3 appear at Times t_1^2 and t_2^2 sequentially. In the meantime, the two loads moved a distance of d that equals the distance between the two loads. Because the velocity of the loads has already been obtained using Eq. (13), d can be calculated as follows:

$$d = v(t_2^1 - t_1^1) \quad \text{or} \quad d = v(t_2^2 - t_1^2) \quad (15)$$

Assuming that, in the previous discussion, each concentrated load represents an axle load, to detect the vehicle speed and the axles, two groups of measurement points are needed. In fact, only four points are need for the two groups of measurement points because the last two points (O_1 and Q_1) in the first group can also be used as the first two points (P_2 and O_2) of the second group.

In-service bridges normally work within the linear-elastic range under routine traffic loads and, therefore, can be considered as linear-elastic structures. Therefore, the global bending

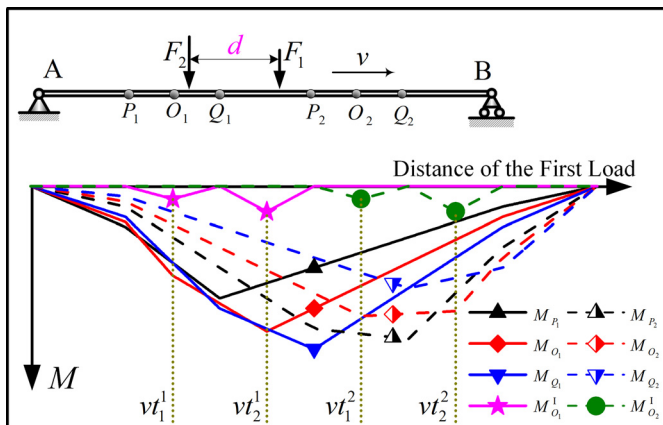


Fig. 3. Moment curves of different measurement points and the isolated moments under two moving loads

moment of a bridge is linearly related to the normal strain of the bridge in the longitudinal direction. Taking a multigirder bridge as an example, the total global bending moment of the bridge at a cross section can be calculated based upon the recorded normal strain (ϵ) as follows:

$$M = \sum_{i=1}^n EW_i \epsilon_i \quad (16)$$

where E = modulus of elasticity of the bridge material; and W_i and ϵ_i = section modulus and normal strain of the i th girder, respectively. However, in this study, it was found that using the strain information from one particular girder that bears a significant portion of vehicle loads can fulfill the requirement of identifying vehicle speed and axle spacing, even under different transverse locations of the moving vehicle. Therefore, there is no need to install sensors on all four girders in the lateral direction, and the strain information from the girder that takes the largest amount of vehicle loads was selected in the present study.

Because this method sets no requirement on the boundary conditions of Beam AB, it is applicable to not only simply supported bridges but also continuous bridges. However, it should be noted that, to clearly detect each axle load, it is ideal that the loads have a space larger than the distance between two adjacent measurement points (i.e., $d > l$). If a vehicle has multiple axles that are spaced very closely (for example, an axle group), the distances between the measurement points should also be set to small values. This may lead to a small value of $M_{O_i}^1$, whose valleys may not be easily identified under noisy conditions. Under such cases, the method may automatically treat the closely spaced axles as one single axle in the identification process, as will be demonstrated in the numerical simulations.

Once the vehicle speed and axle spacing are obtained from the strain information, the Moses algorithm or its derivative methods, which are adopted for most current BWIM systems, can be used to identify the axle weight of the vehicles.

Numerical Simulations

Case Description

To investigate the accuracy and efficiency of the proposed method, numerical simulations were carried out and a series of case studies were conducted. In this study, a simply supported girder bridge with four identical T-beams was adopted. This two-lane bridge has a span length of 20 m and a width of 8.5 m. Fig. 4 shows the cross

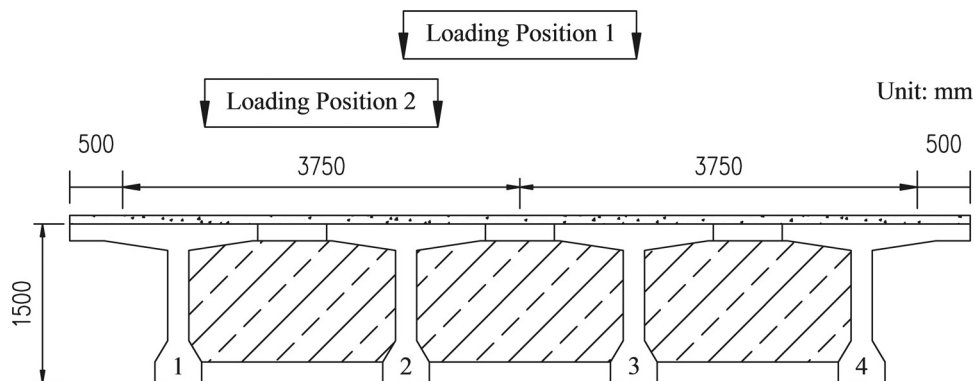


Fig. 4. Bridge cross section and considered loading positions

section of the bridge. Both the cases with a single vehicle and cases with multiple vehicle presence were considered.

Four measurement stations were selected along the bottom of the girders that take a significant portion of vehicle loads. The strain information at these points was used in the identification process. For the purpose of illustration, Fig. 5 shows the four points selected on Girder 2. These four points have a spacing of 2 m between each other in the longitudinal direction. The first Point A is located 8 m from the entrance of the bridge. Fig. 6 shows the ideal influence lines for the strains of the four measurement stations on Girder 2 (ϵ_A , ϵ_B , ϵ_C , and ϵ_D), as well as the strains due to the isolated moments (and, referred to as the isolated strain hereafter) when the truck moves into Loading Position 1, shown in Fig. 4.

In the present study, three different trucks, which represent typical trucks on the road, were used to test the proposed method. The gross weights of the three trucks are 73.5, 320.1, and 392.4 kN, respectively. Fig. 7 shows the axle weight distribution of the three trucks. The analytical models for these three trucks are shown in Fig. 8, where the trucks are represented by a combination of rigid bodies connected by a series of springs and damping devices. The three truck models shown in Fig. 8 were used in the numerical

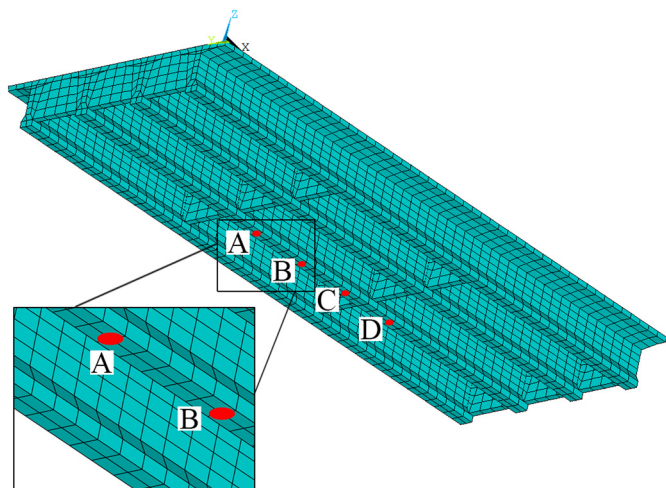


Fig. 5. Bridge finite-element model and locations of the four measurement stations on Girder 2

simulations. These truck models have also been used by many other researchers (Harris et al. 2007; Shi and Cai 2009; Wang and Liu 2000; Zhang et al. 2006; Zhou and Chen 2015). Detailed parameters of the three vehicle models can be found in Harris et al. (2007) and Zhang et al. (2006), respectively. The parameters used in the case studies are summarized in Table 1.

Identification Results for Single-Vehicle Cases

Two loading positions, as shown in Fig. 4, were considered for the single-vehicle cases. The strains measured from the four points on Girder 2 were used for identification. To reduce the noise in the signal that may be introduced by the random road surface roughness or by the measurement system (in the case of measured data), a Butterworth low-pass filter was designed and applied to the strain time histories. An empirical formula for calculating the stopband frequency of the filter is $f_p = 12[v_e/(2L_{\text{Bridge}})]$, where L_{Bridge} is the length of the bridge, and v_e is the velocity of the vehicle. In practice, the vehicle speed could be roughly estimated as follows:

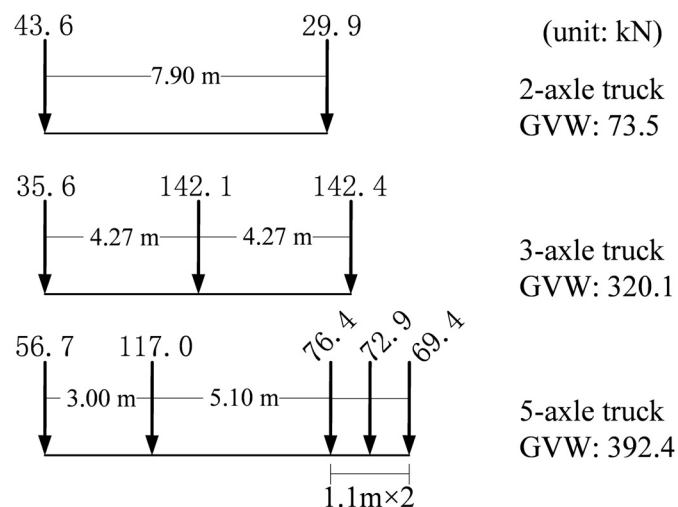


Fig. 7. Static axle load distribution of the three trucks (Note: GVW = gross vehicle weight)

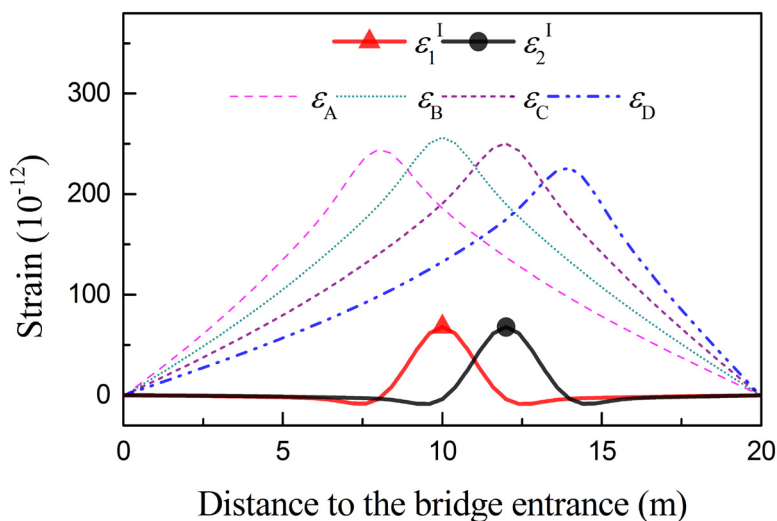


Fig. 6. Strain influence lines of measurement stations (Loading Position 1)

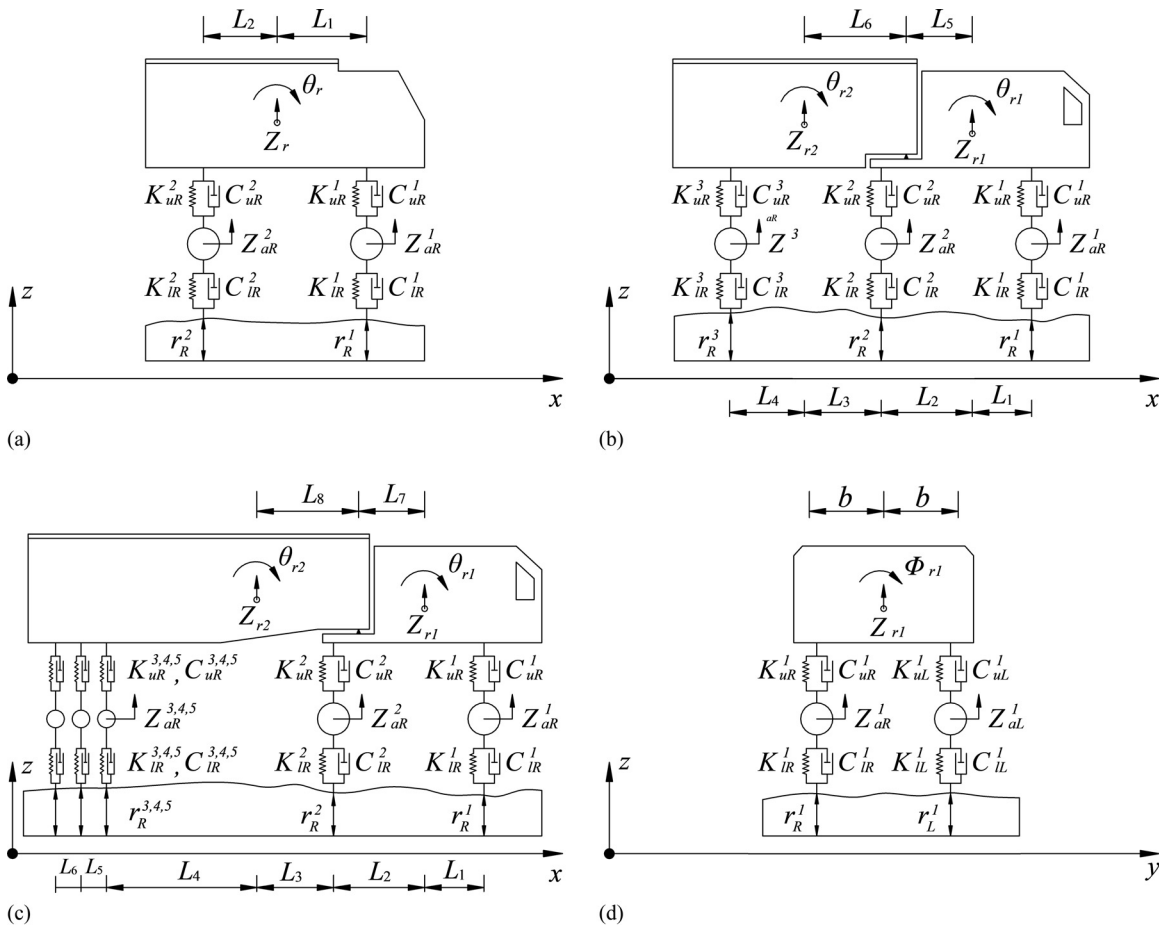


Fig. 8. Analytical models of the three trucks: (a) 2-axle truck; (b) 3-axle truck; (c) 5-axle truck; (d) front view of the trucks

Table 1. Values of Parameters Considered in Case Studies

Parameter	Value
Vehicle speed (m/s)	10, 15, 20, 25, 30
RSC	Smooth, very good, good, average
Truck type	2-axle truck, 3-axle truck, 5-axle truck
Truck loading position	Center of roadway, center of left traffic lane

$v_e = (L_{\text{Bridge}} + \bar{L}_{\text{Truck}})/T$, where \bar{L}_{Truck} is a proper upper bound of the truck length (8.6 m was used in the present study), and T is the time needed for the vehicle to travel across the bridge. In this study, the filtered strain information was then used in the identification process. In addition, to better simulate the measured signals, two levels of white noise (namely, 5 and 10%) were added to the strain signals generated from the numerical simulations, and the effect of noise on the accuracy of the proposed method was investigated.

Figs. 9–11 show the typical flexural strains at Locations A, B, C, and D on Girder 2 and the strains due to the isolated bending moments of the bridge under the passage of each of the three trucks at a speed of 20 m/s. For the sake of brevity, only the results for smooth and average RSCs when the truck was in Loading Position 1 are presented in this paper. For the cases with average RSCs, the filtered strain signals are also plotted using thin solid lines in the same figures, similarly hereafter.

Using the simulated flexural strain time histories as the input, the vehicle speed, axle count, and axle spacing of the vehicles were

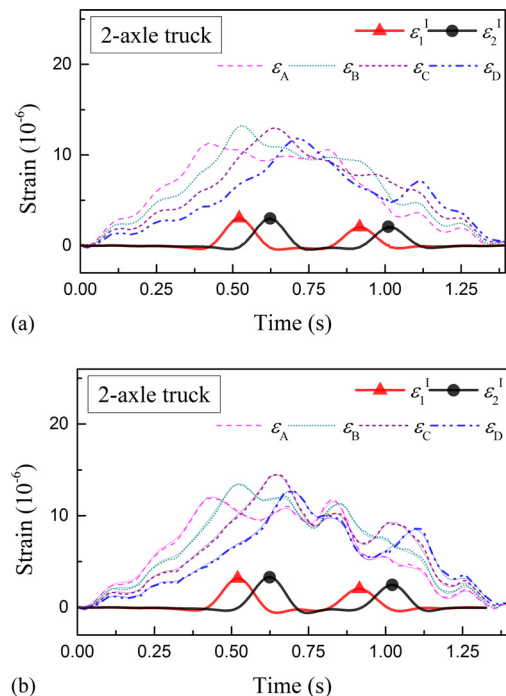


Fig. 9. Simulated strains and detected peaks in isolated strains under different RSCs (Loading Position 1, 2-axle truck, $v = 20$ m/s): (a) smooth RSC; (b) average RSC

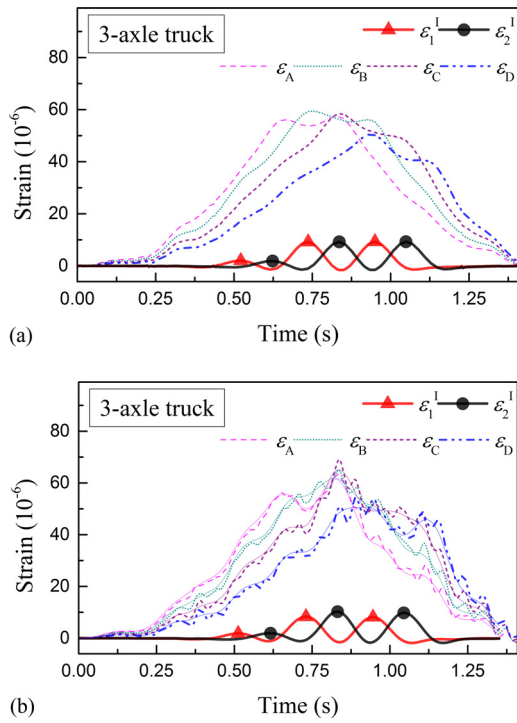


Fig. 10. Simulated strains and detected peaks in isolated strains under different RSCs (Loading Position 1, 3-axle truck, $v = 20$ m/s): (a) smooth RSC; (b) average RSC

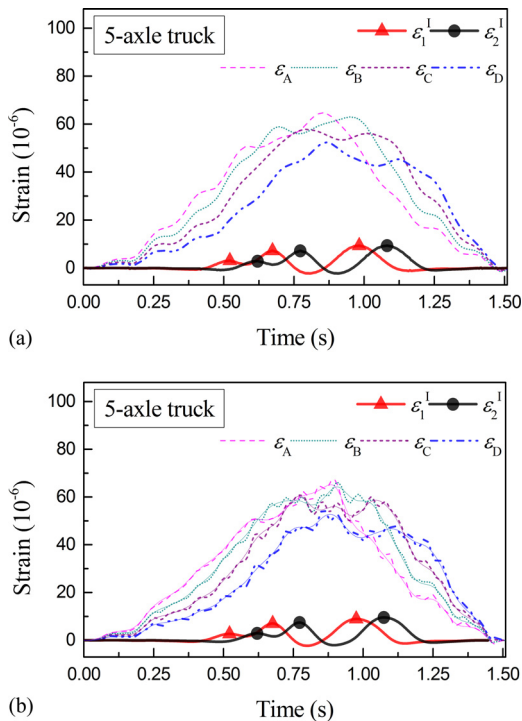


Fig. 11. Simulated strains and detected peaks in isolated strains under different RSCs (Loading Position 1, 5-axle truck, $v = 20$ m/s): (a) smooth RSC; (b) average RSC

estimated using the proposed method. The identified results for all of the single-vehicle cases considered are summarized in Tables 2, 3, and 4 for the 2-, 3-, and 5-axle trucks, respectively. In these three

Table 2. Identification Results and Relative Errors of the 2-Axle Truck (Loading Position 1)

RSC	Vehicle speed			Axle spacing	
	v_0 (m/s)	v_1 (m/s)	Error (%)	AS (m)	Error (%)
Smooth	10	10.00	0.0	7.80	-1.3
	15	14.81	-1.2	7.70	-2.5
	20	19.74	-1.3	7.70	-2.5
	25	24.99	-0.1	7.77	-1.6
	30	30.37	1.2	7.90	0.0
Very good	10	10.00	0.0	7.80	-1.3
	15	14.81	-1.2	7.70	-2.5
	20	19.99	-0.1	7.77	-1.6
	25	25.31	1.2	7.90	0.0
	30	30.37	1.2	7.90	0.0
Good	10	10.13	1.3	7.92	0.3
	15	15.38	2.6	8.00	1.3
	20	19.50	-2.5	7.63	-3.4
	25	24.67	-1.3	7.75	-1.9
	30	29.98	-0.1	7.77	-1.6
Average	10	10.13	1.3	7.92	0.3
	15	16.00	6.7	8.24	4.3
	20	20.78	3.9	8.11	2.6
	25	25.97	3.9	8.11	2.6
	30	29.61	-1.3	7.70	-2.5

Table 3. Identification Results and Relative Errors of the 3-Axle Truck (Loading Position 1)

RSC	Vehicle speed			Axle spacing			
	v_0 (m/s)	v_1 (m/s)	Error (%)	AS1 (m)	Error (%)	AS2 (m)	Error (%)
Smooth	10	10.00	0.0	4.25	-0.4	4.30	0.8
	15	14.81	-1.2	4.22	-1.0	4.22	-1.0
	20	20.07	0.4	4.30	0.7	4.27	0.1
	25	25.31	1.2	4.31	1.0	4.31	1.0
	30	30.37	1.2	4.31	1.0	4.31	1.0
Very good	10	9.68	-3.2	4.16	-2.5	4.19	-1.9
	15	14.81	-1.2	4.26	-0.2	4.33	1.6
	20	19.58	-2.1	4.19	-1.8	4.19	-1.8
	25	24.67	-1.3	4.25	-0.4	4.25	-0.4
	30	30.63	2.1	4.42	3.6	4.40	3.0
Good	10	9.60	-4.0	4.20	-1.6	4.08	-4.4
	15	14.81	-1.2	4.19	-1.9	4.19	-1.9
	20	19.91	-0.5	4.34	1.6	4.18	-1.9
	25	25.31	1.2	4.36	2.2	4.38	2.8
	30	30.90	3.0	4.43	3.9	4.36	2.1
Average	10	9.60	-4.0	4.22	-1.0	4.10	-3.8
	15	15.00	0.0	4.28	0.2	4.46	4.6
	20	19.26	-3.7	4.34	1.7	4.34	1.7
	25	24.88	-0.5	4.44	4.0	4.41	3.4
	30	27.98	-6.7	3.90	-8.7	3.90	-8.7

tables, v_0 and v_1 represent the true and predicted vehicle speeds, respectively; AS represents the axle spacing; and AW and GVW represent the axle weight and gross vehicle weight, respectively. Again, for the sake of brevity, only the results for Loading Position 1 are presented.

Because the three axles in the rear axle group of the 5-axle truck are spaced very closely, it was difficult to clearly identify the peaks

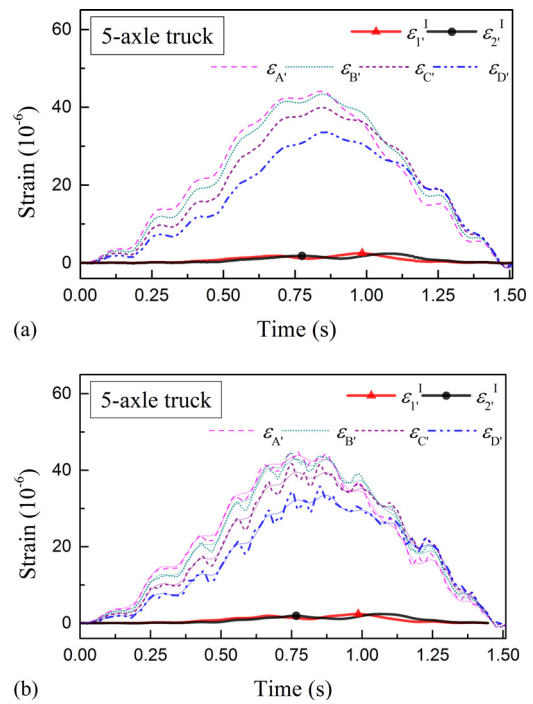
Table 4. Identification Results and Relative Errors of the 5-Axle Truck (Loading Position 1)

RSC	Vehicle speed			Axle spacing			
	v_0 (m/s)	v_1 (m/s)	Error (%)	AS1 (m)	Error (%)	AS2 (m)	Error (%)
Smooth	10	10.00	0.0	2.95	-1.7	5.95	-3.5
	15	15.19	1.3	3.04	1.3	6.04	-2.1
	20	20.60	3.0	3.08	2.6	6.16	-0.1
	25	24.67	-1.3	3.03	0.8	5.88	-4.7
	30	30.37	1.2	3.08	2.6	6.03	-2.3
Very good	10	10.00	0.0	2.95	-1.7	5.95	-3.5
	15	15.19	1.3	3.04	1.3	6.04	-2.1
	20	20.42	2.1	3.10	3.4	6.08	-1.4
	25	24.88	-0.5	3.03	0.8	5.95	-3.5
Good	10	10.08	0.8	2.95	-1.7	6.00	-2.7
	15	15.38	2.6	3.08	2.6	6.08	-1.4
	20	20.07	0.4	3.10	3.4	6.00	-2.7
	25	25.52	2.1	3.10	3.4	6.08	-1.4
Average	10	10.26	2.6	3.03	0.9	6.10	-1.0
	15	15.19	1.3	3.04	1.3	6.00	-2.7
	20	20.25	1.2	3.08	2.6	6.05	-1.8
	25	24.47	-2.1	2.98	-0.8	5.83	-5.5
	30	29.86	-0.5	3.05	1.7	5.80	-5.9

on the isolated strains caused by the passage of each individual axle, as can be seen from Fig. 11, in which only three obvious peaks are observed, which correspond to the passage of the front axle, second axle, and rear axle group of the 5-axle truck. It has been reported to be pragmatic that closely spaced axles forming an axle group are identified as a single axle in practice, because accurately identifying the weights of closely spaced axles is very difficult (O'Brien et al. 2009; WAVE 2001). As a result, the three axles in the rear axle group were treated as a single axle in the identification process. In this way, the true weight for the equivalent rear axle of the 5-axle truck is 218.7 kN, which is the total weight of the three axles in the rear, and the axle spacing between the second axle and the equivalent rear axle is 6.165 m, which is measured from the middle of the rear axle group.

From Tables 2, 3, and 4, the following can be observed: (1) the relative errors for the identified vehicle speed and axle spacing are less than 5% in most cases; (2) the vehicle type and vehicle speed seem to have a negligible effect on the accuracy of the identified results; and (3) the road surface condition seems to have a small influence on the accuracy of the identified results, as can be seen from the fact that the errors increase slightly as the road surface condition becomes worse; however, the relative errors are generally under 5%, even under average RSCs.

In addition to the effects of the previously discussed factors, the effects of vehicle loading position and selection of measurement stations on the accuracy of the proposed method were also investigated. Although the detailed results are not presented here for the sake of brevity, the results show that the same level of accuracy can be achieved under the two different loading positions investigated when the strain signals from Girder 2 are used. This is because Girder 2 takes a significant portion of vehicle loads under both loading conditions. To investigate the effect of the measurement stations, the flexural strains of another four points under Girder 3 were used in the identification process. For the purpose of illustration, only the results for the 5-axle truck traveling at a speed of 20 m/s under smooth and average RSCs are presented in Fig. 12 and

**Fig. 12.** Simulated strains and detected peaks in isolated strains on Girder 3 (Loading Position 2, 5-axle truck, $v = 20$ m/s): (a) smooth RSC; (b) average RSC**Table 5.** Relative Identification Errors Using Strains on Girder 3

Truck	RSC	Loading Position 1 (%)			Loading Position 2 (%)		
		Speed	AS1	AS2	Speed	AS1	AS2
5-axle	Smooth	0.0	0.0	0.6	-10.4	11.9	-10.7
	Average	5.3	8.8	2.4	-1.6	100.0	-7.5

Table 5. Fig. 12 shows that the isolated strain curves obtained from Girder 3 when the 5-axle truck travels along Loading Position 2 do not show peaks as clear as those under Loading Position 1, as shown in Fig. 11, leading to much larger identification errors, as shown in Table 5. Therefore, to achieve better identification accuracy, it is better to set the measurement stations directly underneath the loaded lane.

The effect of noise in the input signals on the accuracy of the identified results was also investigated. To simulate the noise, the original strain signals were polluted with 5 and 10% white noise. To avoid the bias caused by the random road surface profile generated in the numerical simulation, for each specific case, 10 random road surface profiles were generated, and the bridge-vehicle coupled program was set to run 10 times independently, resulting in 10 identified results and identification errors. The mean value and standard deviation of the 10 identification errors were then used in the error analysis.

Fig. 13 shows the identification errors of vehicle speed and axle spacing of the trucks under various noise levels. In these figures, the solid lines denote the smooth RSC, and the dashed lines denote average RSC. In general, the relative errors and standard deviations under smooth RSCs are smaller than those under average RSCs. Fig. 13 shows that the mean identification errors of vehicle speed and axle spacing are within 5% under all conditions, and that the mean identification errors and standard

deviations only increase slightly as the noise level increases from 0 to 10%, indicating that the proposed method is robust under noisy conditions. This is possibly due to the fact that the influence of noise has been largely removed by the Butterworth low-pass filter, making the peaks more identifiable by the proposed method.

Identification Results for Cases with Multiple Truck Presence

Cases with a multiple truck presence were also investigated. Loading scenarios with a 2-axle truck traveling in Lane 1 and a 3-axle truck traveling in Lane 2 at the same time were considered, as illustrated in Fig. 14. Different relative longitudinal positions

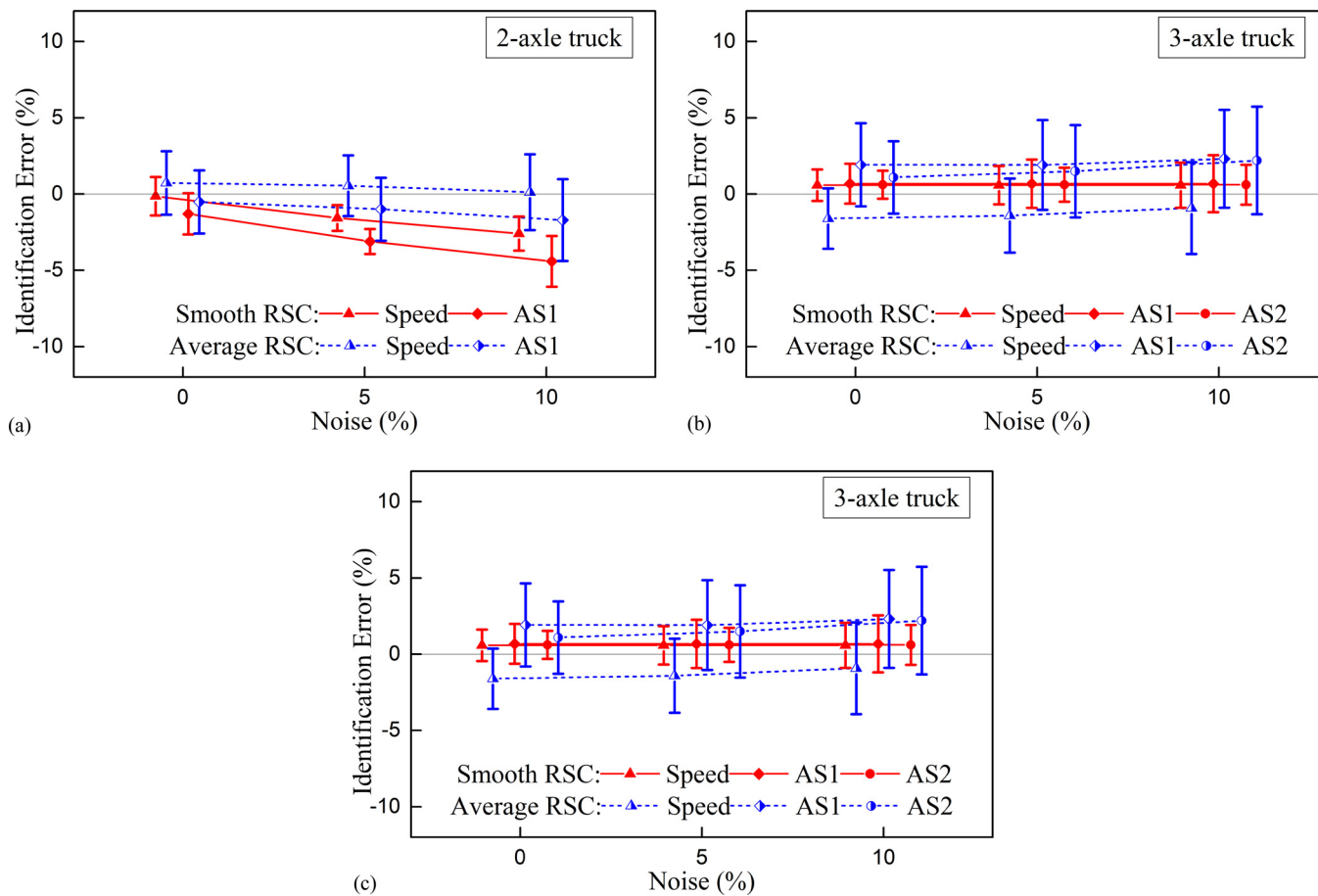


Fig. 13. Mean and standard deviation of identification errors of vehicle speed and axle spacing under various noise levels: (a) 2-axle truck; (b) 3-axle truck; (c) 5-axle truck (Note: Solid line = smooth RSC; dashed line = average RSC)

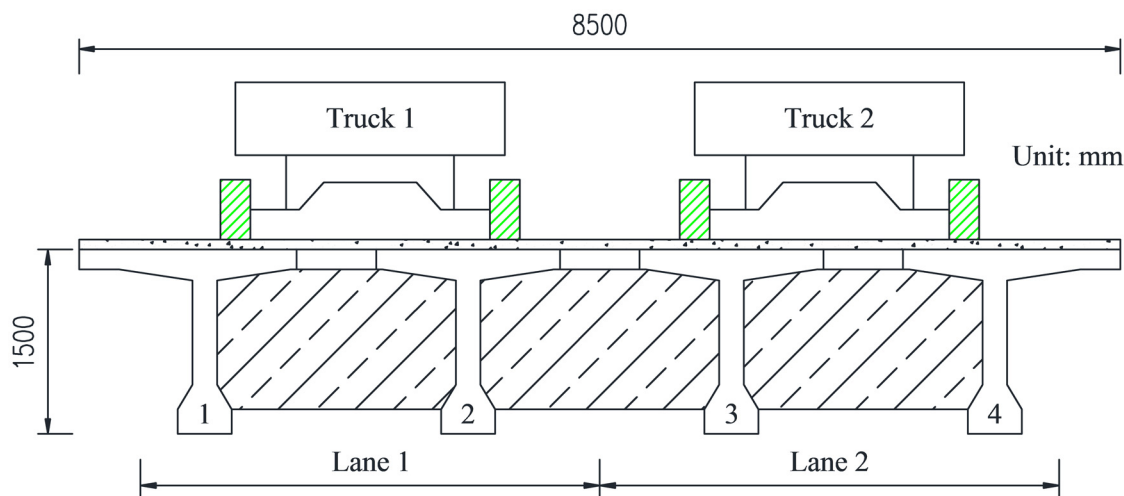


Fig. 14. Cases with multiple truck presence

of the two trucks were also considered, and three cases were investigated in which the head-to-head distance (in the longitudinal direction) of the two trucks was set to 0 m (i.e., two trucks side by side), 5 m, and 10 m, respectively. With each relative truck position, five vehicle speeds were investigated. The identification procedure for identifying vehicle speed and axles was the same as that used in the single-vehicle cases. The only difference was that the axles of each truck were identified using the bridge response of the girder that is closer to the truck (i.e., the parameters of Truck 1 and Truck 2 were identified using the strains of Girder 2 and Girder 3, respectively).

The identification results under average RSCs are summarized in Table 6. Table 6 shows that good accuracy was achieved in the identified vehicle speed and axles for both trucks under all cases studied. For the purpose of illustration, Fig. 15 plots the simulated bridge strain time histories of Girder 2 and Girder 3 and the isolated strains when the two trucks passed through the bridge at a speed of 20 m/s. The RSC used in this case was average, and the head-to-head distance of the two trucks was set to 5 m. Fig. 15 shows that the peaks in the isolated strain time histories for both girders can still be clearly identified when two trucks were present on the bridge at the same time.

The cases with the two vehicles traveling at different speeds were also investigated. In the cases considered, the speed of the 2-axle truck was kept at 20 m/s, whereas five different speeds (from 10 to 30 m/s) were considered for the 3-axle truck. The two trucks were assumed to enter the bridge at the same time in all cases investigated, and an average RSC was adopted. The identification results are summarized in Table 7. This table shows that the proposed method can successfully identify the vehicle speed and the axles of both trucks with good accuracy, even though the two trucks were traveling at different speeds.

Experimental Validation

In addition to the numerical simulations performed in the previous section, experimental studies were also conducted in the laboratory to verify the effectiveness and accuracy of the proposed VSSB method. Only the single-vehicle cases were investigated in the experiments.

Experimental Setup

Fig. 16 shows the test platform developed in the laboratory. To run a test, the vehicle model is first hauled to a certain height on the ramp by a rope. Then, the rope is released and the vehicle model travels down along the rail under the effect of gravity and gains a certain speed before entering the test bridge model. The vehicle speed can be adjusted by adjusting the original position of the vehicle on the ramp. The transverse loading position of the vehicle on the bridge model can also be adjusted by adjusting the transverse position of the rail or the lateral position of the bridge model.

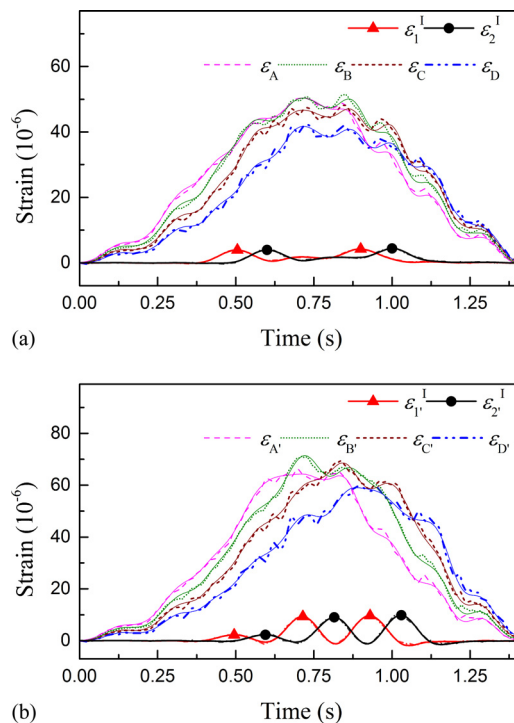


Fig. 15. Simulated strains and detected peaks in the isolated strains (average RSC, $v = 20$ m/s, head-to-head distance = 5 m): (a) Girder 2; (b) Girder 3

Table 6. Identification Results and Relative Errors of Two Trucks Traveling at the Same Speed

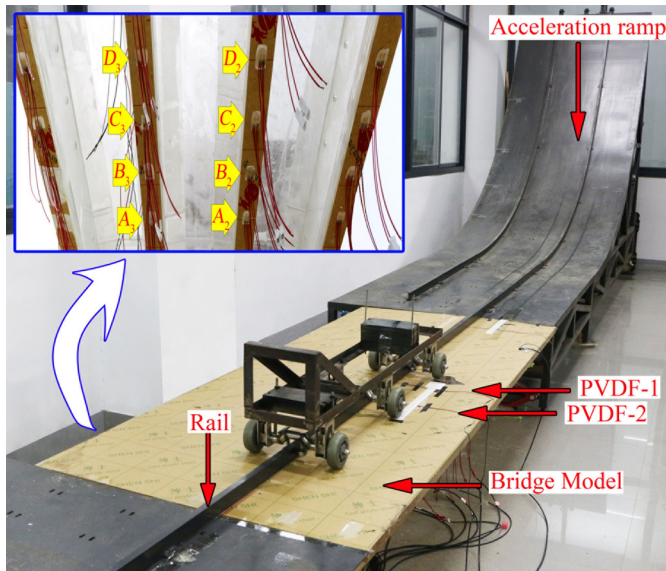
Head-to-head distance (m)	v_0 (m/s)	2-Axle truck		3-Axle truck		
		v_1 (m/s)	AS1 (m)	v_1 (m/s)	AS1 (m)	AS2 (m)
0	10	10.05 (0.5)	8.00 (1.3)	10.00 (0.0)	4.35 (1.9)	4.30 (0.8)
	15	14.84 (-1.0)	7.82 (-1.1)	14.84 (-1.0)	4.27 (0.2)	4.25 (-0.3)
	20	20.00 (0.0)	7.95 (0.6)	20.00 (0.0)	4.40 (3.0)	4.28 (0.3)
	25	25.92 (3.7)	8.27 (4.7)	25.00 (0.0)	4.37 (2.4)	4.29 (0.5)
	30	30.66 (2.2)	8.16 (3.3)	30.77 (2.6)	4.46 (4.5)	4.43 (3.9)
5	10	10.00 (0.0)	8.13 (2.9)	9.99 (-0.1)	4.34 (1.7)	4.31 (0.9)
	15	14.81 (-1.2)	8.05 (1.9)	14.87 (-0.9)	4.27 (0.2)	4.28 (0.4)
	20	20.00 (0.0)	8.13 (3.0)	20.00 (0.0)	4.40 (3.0)	4.28 (0.4)
	25	25.00 (0.0)	8.12 (2.7)	25.00 (0.0)	4.34 (1.8)	4.33 (1.4)
	30	29.89 (-0.4)	8.09 (2.5)	30.77 (2.6)	4.43 (3.9)	4.41 (3.3)
10	10	10.00 (0.0)	7.99 (1.1)	10.00 (0.0)	4.39 (3.0)	4.31 (1.0)
	15	14.81 (-1.2)	7.93 (0.4)	14.87 (-0.9)	4.34 (1.9)	4.26 (-0.2)
	20	20.00 (0.0)	7.97 (0.9)	20.00 (0.0)	4.43 (3.9)	4.28 (0.3)
	25	25.00 (0.0)	8.00 (1.3)	25.00 (0.0)	4.43 (3.9)	4.31 (1.0)
	30	30.66 (2.2)	8.19 (3.6)	30.77 (2.6)	4.53 (6.2)	4.39 (3.0)

Note: Values in parentheses denote the relative difference (%) between the identified values and their true values.

Table 7. Identification Results and Relative Errors of the Two Trucks Traveling at Different Speeds

Speed of Truck 2 (m/s)	2-Axle truck		3-Axle truck		
	v_1 (m/s)	AS (m)	v_1 (m/s)	AS1 (m)	AS2 (m)
10	20.00 (0.0)	8.13 (2.9)	10.00 (0.0)	4.40 (3.0)	4.31 (1.1)
15	20.00 (0.0)	8.04 (1.8)	14.81 (-1.2)	4.26 (-0.1)	4.27 (0.0)
20	20.00 (0.0)	7.95 (0.6)	20.00 (0.0)	4.40 (3.0)	4.28 (0.3)
25	20.00 (0.0)	7.68 (-2.8)	25.00 (0.0)	4.35 (2.0)	4.33 (1.4)
30	20.63 (3.2)	8.19 (3.7)	30.77 (2.6)	4.46 (4.6)	4.40 (3.2)

Note: Values in parentheses denote the relative difference (%) between the identified values and their true values.

**Fig. 16.** Test platform

Because of the limited height of the ramp, the tested vehicle speed was limited to a maximum of approximately 5 m/s, which corresponds to a speed of 52 km/h for a full-scale vehicle.

Based on the bridge model adopted in the “Numerical Simulations” section and similar principles, a bridge model was built in the laboratory. This scaled bridge model is a simply supported multigirder bridge with a scale ratio of 1:0.119. It has a total length of 2.38 m and a width of 1.01 m. The bridge model is made with polymethyl methacrylate (PMMA) material, which has a Young’s modulus of 2,795 MPa and density of 1,181.6 kg/m³. Detailed ratios of similitude for this bridge model to the original bridge model in Fig. 16 are summarized in Table 8.

The cross section of the scaled bridge model is illustrated in Fig. 17. The cross section was slightly modified from the original bridge cross section for convenience during manufacturing. Fig. 17 also shows the lanes and the lateral loading position of the truck model in the experiments.

As can be seen from Fig. 17, this bridge model has four I-girders. Four foil strain gauges were installed under each of the interior girders (i.e., G2 and G3). Fig. 18 shows the sensor positions on each girder. As discussed earlier, the four sensors on each girder can serve two VSSBs centered about Point B and Point C, respectively. In addition, two polyvinylidene fluoride (PVDF) cables were mounted to the deck surface in the transverse direction. These PVDF cables were used to identify the vehicle speed, which was then used to validate the results obtained from the proposed VSSB method. When a vehicle axle passes through the

Table 8. Ratios of Similitude of Bridge Model

Description	Similitude ratio
Dimension (L)	0.119
Young modulus (E)	0.081
Strain (ϵ)	1
Stress (σ)	0.081
Deflection (δ)	0.119
Moment of inertia of cross section (I)	2.01×10^{-4}
Area (A)	0.014
Mass (M)	1.15×10^{-3}
Stiffness (K)	9.64×10^{-3}
Natural frequency (ω)	2.899
Vehicle speed (v)	0.345
Loads (F)	1.15×10^{-3}

PVDF cable, the pressure exerted on the cable generates an impulse noting the passage of the axle. Based on the time lag between the impulses generated by the same axle passing through the two PVDF cables and the distance between the two cables, the vehicle speed can be determined.

A 248-kN 3-axle truck was used as the original truck for the scaled vehicle model, which is shown in Fig. 19. This vehicle model was mainly made of steel components. It consists of two vehicle bodies connected through a hinge. The masses of the vehicle bodies and their mass centers can be adapted by adding/removing steel plates and adjusting the positions of the steel plates. The position of the three axles can also be adjusted. The suspension systems of the axles were simulated by springs whose stiffness can also be adjusted. Table 9 shows the key parameters of the truck model used in the present study.

To study the effect of vehicle loading position on the accuracy of the proposed method, three truck loading positions, in the transverse direction, were adopted. Because the bridge is symmetric about the centerline, only Lane 1 was investigated. Under the three cases, the truck travels across the bridge along the left edge of Lane 1, the center of Lane 1, and the right edge of Lane 1, respectively. In addition, the effect of vehicle speed was also investigated. Because of the limitation of the experimental platform as discussed at the beginning of this section, the tested vehicle speed was set within a range of 1–5 m/s, which corresponds to a range of 2.9–14.5 m/s (10.4–52.2 km/h) for a full-scale truck according to a similar principle.

Result Analysis

To verify the proposed method, a series of test cases were examined. For the purpose of illustration, Fig. 20 shows the results of a test series in which the vehicle traveled across the bridge along different transverse positions at a speed of approximately 3 m/s.

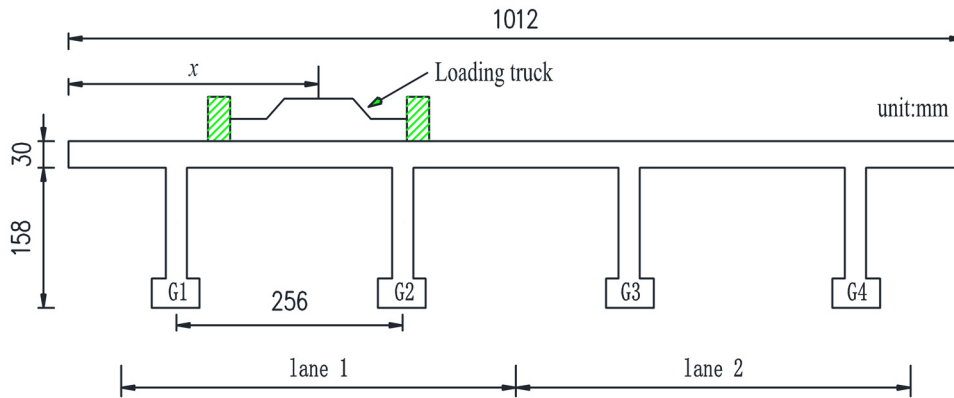


Fig. 17. Cross section of scaled bridge model and truck loading position

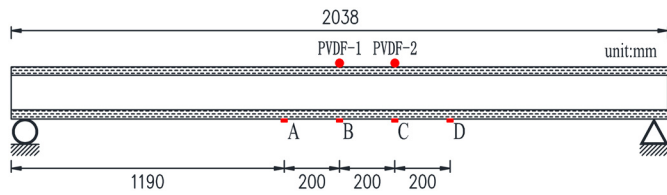


Fig. 18. Side view of scaled bridge model and sensor positions

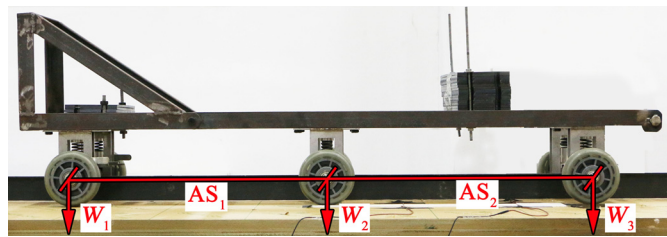


Fig. 19. Scaled 3-axle truck model

Table 9. Axle Spacing and Weight Distribution for Truck Model

AS1 [mm (m)]	AS2 [mm (m)]	W ₁ [kg (kN)]	W ₂ [kg (kN)]	W ₃ [kg (kN)]
454.0 (3.82)	472.1 (3.97)	8.998 (76.83)	13.972 (119.36)	6.070 (51.84)

Note: Values in parentheses are the corresponding values for the original full-scale truck model according to the similar principle.

In Fig. 20, the strain time histories obtained from the four sensors and the calculated isolated strains on each of the three instrumented girders are plotted. Also included in Fig. 20 are the signals from the PVDF cables, which can be used to directly identify the passage of vehicle axles.

As can be seen from Fig. 20, the calculated isolated strain signals on both Girders 2 and 3 clearly show three peaks that correspond to the passage of the three axles. Therefore, the strains on either of the two girders can be used to identify the axle information. Because the bridge is symmetric about the centerline, to successfully identify the axle information of the truck traveling in either traffic lane, only two girders need to be instrumented. However, it was also noticed that Girder 1 failed to show such obvious peaks

when the truck traveled along the right edge of Lane 1 because Girder 1 was far away from the truck loading position.

Table 10 summarizes the identification results, using both the proposed VSSB method and the PVDF cables, for the test cases conducted. The strain on Girder 2 was used for the VSSB method in all cases. The true axle distances of the truck model are shown in Table 11. The truck speeds identified by the PVDF cables were treated as the true values and were used for validation of the proposed method.

Table 10 shows that, under different vehicle speeds and vehicle lateral loading positions, both methods can achieve good accuracy for the identified axle distances, with the relative errors falling within 5% for most cases. It is also observed that the results identified using the PVDF cables are not necessarily more accurate than those identified using the VSSB method. In addition, it is observed that the relative differences between the identified vehicle speeds using the two methods are all within 5%, except for one case, indicating that the proposed VSSB has good accuracy.

Compared with the FAD method, although the proposed VSSB method needs to install one more strain sensor for each traffic lane, it has the following distinct advantages. First, unlike the existing FAD methods, the proposed VSSB method is not limited to the type of boundary conditions or the length of the bridge. Neither is it limited to slab bridges with relative thick deck or slab-on-girder bridges. Second, the isolated strain is sensitive to the axle passage for a wide range of vehicle lateral positions. As demonstrated by the results in Table 10, the strains on Girder 2 can be used to successfully identify the axle information under different vehicle lateral positions investigated.

The effect of axle spacing on the effectiveness and accuracy of the proposed method was also investigated. In addition to tested truck configuration, three other axle spacing schemes, as shown in Table 11, were also investigated. For convenience, the corresponding truck models with different axle spacings are hereafter referred to as Model 2, Model 3, and Model 4, respectively.

Figs. 21(a–c) shows the measured strains as well as the signals from the PVDF cables when each of the three truck models traveled across the bridge along the right edge of Lane 1 at a speed of approximately 2 m/s. The isolated strains and measured signals from the PVDF cables are also plotted. Fig. 21(a) shows that, with a rear axle spacing of 312 mm, the isolated strain curves for Truck Model 2 clearly show three peaks. In contrast, with a reduced rear axle spacing in Truck Model 3, the three peaks are still identifiable but with increasing difficulty, as shown in Fig. 21(b). With a further reduced rear axle spacing of 207 mm, which is close to the sensor spacing, only two obvious peaks can

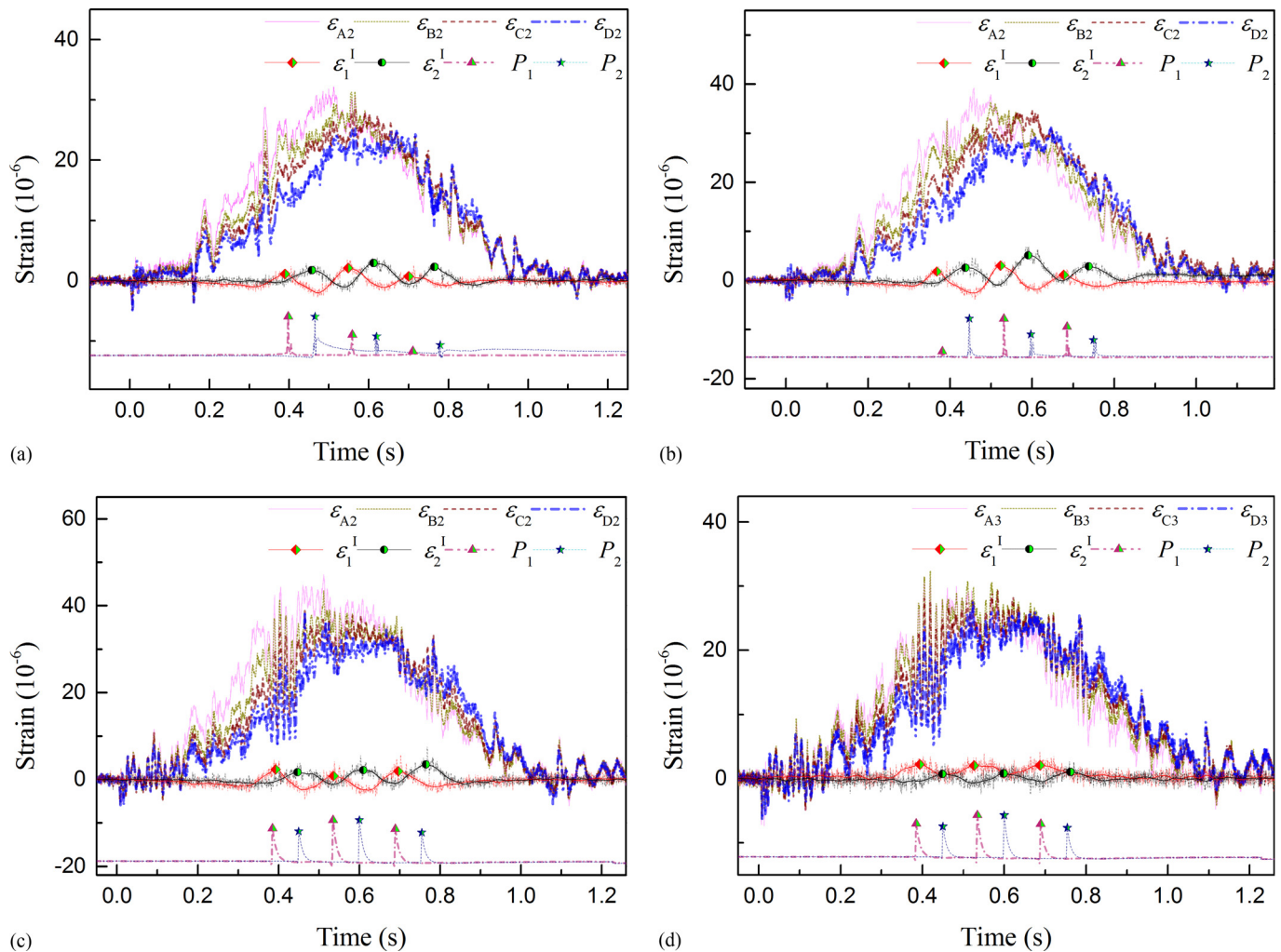


Fig. 20. Measured strains for different cases (Note: speed in parentheses is the corresponding speed for full-scale truck): (a) G2, left edge of Lane 1, 3.05 m/s (31.78 km/h); (b) G2, center of Lane 1, 3.05 m/s (31.87 km/h); (c) G2, right edge of Lane 1, 3.07 m/s (32.03 km/h); (d) G3, right edge of Lane 1, 3.07 m/s (32.03 km/h)

Table 10. Identification Results and Relative Errors

Vehicle lateral position	PVDF				VSSB (G2)		
	v^P (m/s)	$v^{\text{full-scale}}$ (km/h)	AS_1^P (mm)	AS_2^P (mm)	v^V (m/s)	AS_1^V (mm)	AS_2^V (mm)
Left edge of Lane 1	1.00	10.45	442.0 (-2.6)	479.0 (1.5)	1.00 (-0.7)	445.3 (-1.9)	470.1 (-0.4)
	2.07	21.59	447.4 (-1.5)	468.1 (-0.8)	2.12 (2.7)	461.4 (1.6)	483.2 (2.4)
	3.05	31.78	480.5 (5.8)	474.4 (0.5)	3.06 (0.5)	479.8 (5.7)	466.1 (-1.3)
	4.04	42.17	449.5 (-1.0)	471.7 (-0.1)	4.11 (1.7)	458.2 (0.9)	482.9 (2.3)
	5.02	52.40	453.1 (-0.2)	478.2 (1.3)	4.76 (-5.2)	439.3 (-3.2)	452.4 (-4.2)
Center of Lane 1	0.97	10.11	441.6 (-2.7)	476.8 (1.0)	0.98 (0.8)	448.4 (-1.2)	479.7 (1.6)
	2.04	21.26	450.3 (-0.8)	474.2 (0.5)	2.03 (-0.2)	450.0 (-0.9)	471.4 (-0.1)
	3.05	31.87	458.0 (0.9)	467.9 (-0.9)	3.03 (-0.8)	468.2 (3.1)	456.8 (-3.2)
	3.97	41.47	443.0 (-2.4)	451.0 (-4.5)	4.01 (1.0)	418.4 (-7.8)	473.6 (0.3)
	5.13	53.52	451.3 (-0.6)	473.1 (0.2)	4.96 (-3.3)	443.8 (-2.2)	462.4 (-2.0)
Right edge of Lane 1	1.03	10.74	452.8 (-0.3)	486.5 (3.1)	1.00 (-2.9)	434.9 (-4.2)	479.1 (1.5)
	2.07	21.59	456.7 (0.6)	484.7 (2.7)	1.98 (-4.1)	430.4 (-5.2)	464.1 (-1.7)
	3.07	32.03	460.4 (1.4)	473.4 (0.3)	3.05 (-0.5)	467.2 (2.9)	481.7 (2.1)
	4.07	42.45	461.7 (1.7)	487.1 (3.2)	4.11 (1.0)	473.6 (4.3)	493.2 (4.5)
	5.06	52.84	470.9 (3.7)	501.3 (6.2)	5.04 (-0.4)	455.0 (0.2)	521.8 (10.6)

Note: Vehicle speeds identified using PVDF cable are regarded as true values, and the values in parentheses denote the relative difference (%) between the identified values and their true values.

be identified on the isolated strain curves for Truck Model 4, as shown in Fig. 21(c). This was likely because the middle axle and the rear axle were identified as one single-axle group by the

Table 11. Different Axle Spacing Schemes Tested

Truck Model	AS1 [mm (m)]	AS2 [mm (m)]
2	612.0 (5.14)	312.0 (2.62)
3	662.0 (5.56)	262.0 (2.20)
4	709.1 (5.96)	207.5 (1.74)

Note: Values in parentheses are the corresponding values for the original full-scale truck model according to the similar principle.

VSSB method, and the corresponding axle position was taken as the static equivalent position of the two axles. This could be explained as follows. The influence line of the bending moment on an ideal simply supported beam is composed of two segmented straight lines, as shown in Fig. 1(b). Based on the linear beam theory, it can be easily deduced that only one local peak will appear on the isolated moment history when two loads with a distance shorter than the sensor spacing move through the virtual simply supported beam. Under this circumstance, the two loads will be treated as one single load by the proposed method.

Table 12 summarizes the identified results for the three test cases investigated. As can be seen, the proposed method can identify the vehicle speed and axle spacing with good accuracy, except for Truck

Table 12. Test Results for Truck Models with Different Axle Spacings

Truck Model	PVDF				VSSB(G2)		
	v^P (m/s)	$v^{\text{full-scale}}$ (km/h)	AS_1^P (mm)	AS_2^P (mm)	v^V (m/s)	AS_1^V (mm)	AS_2^V (mm)
2	1.92	20.00	587.5 (-4.0)	312.9 (0.3)	1.90 (-0.8)	581.5 (-5.0)	307.1 (-1.6)
3	1.94	20.26	650.5 (-1.7)	258.7 (-1.2)	1.96 (0.8)	663.1 (0.2)	256.9 (-1.9)
4	1.99	20.80	720.1 (1.6)	207.8 (0.1)	2.04 (2.4)	807.1 (2.5) ^a	

Note: Values in parentheses denote the relative difference (%) between the identified values and their true values.

^aEquivalent axle spacing between the front axle and the rear axle group [the true value is calculated to be 787.4 mm using Eq. (17)].

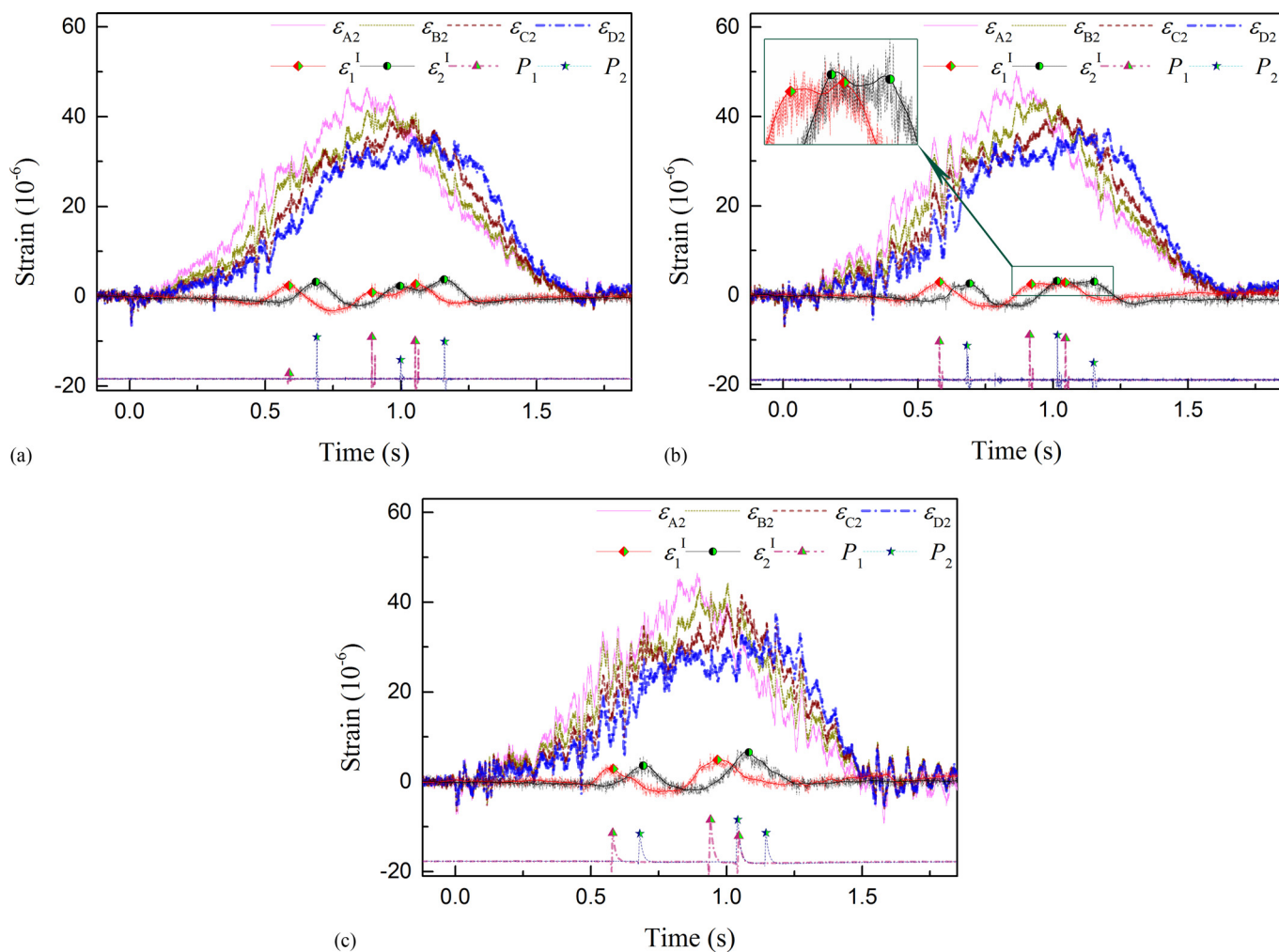


Fig. 21. Measured strains and PVDF signals when the truck model travels along the right edge of Lane 1: (a) Truck Model 2; (b) Truck Model 3; (c) Truck Model 4

Model 4, for which the middle and rear axles were identified as one single axle, whereas the identified axle spacing is very close to the true distance between the first axle and the equivalent static axle for the middle and rear axles. The equivalent axle spacing between the front axle and the rear axle group is calculated as follows:

$$AS = AS_1 + \frac{W_3}{W_2 + W_3} \times AS_2 \quad (17)$$

Summary and Conclusions

For most BWIM techniques, vehicle speed and axle spacing are the prerequisites for identifying the vehicle axle weights. Besides the weighing sensors, additional devices are usually needed to identify the vehicle speed and axle spacing before identifying the axle weights. A novel VSSB method that can utilize the strain signals measured from the weighing sensors to identify the speed and axle spacing of passing vehicles was proposed in the present study. To illustrate the proposed method, numerical simulations were performed using a simply supported girder bridge and three types of trucks. Model tests were also conducted on a scaled bridge model built in the laboratory. The results from both numerical simulations and model tests show that the proposed method can successfully identify the vehicle speed and axle spacing with good accuracy, and the method is not susceptible to noise.

One significant advantage of the proposed method is that it can utilize the weighing sensors to detect the vehicle axles and, therefore, achieve all of the functions of a BWIM system, making it more convenient than most existing BWIM systems. In addition, by adopting the VSSB, which sets no requirement on the boundary condition, this method is applicable not only to simply supported bridges but also to continuous bridges. However, it should be noted that the proposed method may fail to identify closely spaced axles and treats these axles as one single axle under such conditions.

The proposed method assumes that vehicles cross the bridge at constant speeds. Also, this method was only tested on T-beam bridges in the present study because the main focus of this study was to introduce the proposed method. The reliability of the proposed method with respect to other types of bridges, such as slab bridges, will be investigated in future studies. Because the global bending moment is the dominant internal force for many other types of bridges, it is expected that the proposed method would work well on other types of bridges as well. However, for bridges with relative weak transverse connections, the optimal sensor locations should be investigated.

Acknowledgments

The authors acknowledge the financial support provided by the National Natural Science Foundation of China (Grant 51478176) and the funding provided by the Hunan Communications Research Institute.

References

Bao, T., Babanajad, S. K., Taylor, T., and Ansari, F. (2016). "Generalized method and monitoring technique for shear-strain-based bridge weigh-in-motion." *J. Bridge Eng.*, [10.1061/\(ASCE\)BE.1943-5592.0000782](#), 04015029.

Cai, C. S., Shi, X., Araujo, M. S., and Chen, S. (2007). "Influence of approach span conditions on vehicle-induced dynamic response of slab-on-girder

bridges: Field and numerical simulations." *Proc., Transportation Research Board 86th Annual Meeting*, Transportation Research Board, Washington, DC.

Chatterjee, P., Obrien, E., Li, Y., and González, A. (2006). "Wavelet domain analysis for identification of vehicle axles from bridge measurements." *Comput. Struct.*, [84\(28\)](#), 1792–1801.

Deng, L., and Cai, C. S. (2010). "Identification of dynamic vehicular axle loads: Theory and simulations." *J. Vib. Control*, [16\(14\)](#), 2167–2194.

Deng, L., and Cai, C. S. (2011). "Identification of dynamic vehicular axle loads: Demonstration by a field study." *J. Vib. Control*, [17\(2\)](#), 183–195.

Dodds, C. J., and Robson, J. D. (1973). "The description of road surface roughness." *J. Sound Vib.*, [31\(2\)](#), 175–183.

Dunne, D., Obrien, E. J., Basu, B., and Gonzalez, A. (2005). "Bridge WIM systems with nothing on the road (NOR)." *Proc., 4th Int. Conf. on Weigh-In-Motion*, National Science Council, Taipei, Taiwan.

Feng, D. M., and Feng, M. Q. (2015). "Model updating of railway bridge using in situ dynamic displacement measurement under trainloads." *J. Bridge Eng.*, [10.1061/\(ASCE\)BE.1943-5592.0000765](#), 04015019.

Feng, D. M., Sun, H., and Feng, M. Q. (2015). "Simultaneous identification of bridge structural parameters and vehicle loads." *Comput. Struct.*, [157](#), 76–88.

Fryba, L. (1999). *Vibration of solids and structures under moving loads*, Thomas Telford, London.

Harris, N. K., Obrien, E. J., and González, A. (2007). "Reduction of bridge dynamic amplification through adjustment of vehicle suspension damping." *J. Sound Vib.*, [302\(3\)](#), 471–485.

Huang, D., and Wang, T. L. (1992). "Impact analysis of cable-stayed bridges." *Comput. Struct.*, [43\(5\)](#), 897–908.

ISO (International Organization for Standardization). (1995). "Mechanical vibration-road surface profiles-reporting of measured data." *ISO-8608*, Geneva.

Jacob, B., and Obrien, E. J. (1998). "European specification on weigh-in-motion of road vehicles (cost323)." *Proc., 2nd European Conf. on Weigh-in-Motion of Road Vehicles*, Office for Official Publications of the European Communities, Luxembourg.

Kalin, J., Žnidarič, A., and Lavrič, I. (2006). "Practical implementation of nothing-on-the-road bridge weigh-in-motion system." *Proc., Int. Symp. on Heavy Vehicle Weights and Dimensions*, Transportation Association of Canada, Ottawa.

Law, S. S., Chan, T. H. T., and Zeng, Q. H. (1997). "Moving force identification: A time domain method." *J. Sound Vib.*, [201\(1\)](#), 1–22.

Lydon, M., Taylor, S. E., Robinson, D., Mufti, A., and Brien, E. J. O. (2015). "Recent developments in bridge weigh in motion (B-WIM)." *J. Civ. Struct. Health Monit.*, 1–13.

MATLAB [Computer software]. MathWorks, Natick, MA.

Moses, F. (1979). "Weigh-in-motion system using instrumented bridges." *Transp. Engrg. J.*, [105\(3\)](#), 233–249.

O'Brien, E., Hajialzadeh, D., Uddin, N., Robinson, D., and Opitz, R. (2012). "Strategies for axle detection in bridge weigh-in-motion systems." *Proc., 6th Int. Conf. on Weigh-In-Motion (ICWIM 6)*, Wiley-ISTE, London.

O'Brien, E. J., Rowley, C. W., Gonzalez, A., and Green, M. F. (2009). "A regularised solution to the bridge weigh-in-motion equations." *Int. J. Heavy Veh. Syst.*, [16\(3\)](#), 310–327.

O'Brien, E. J., Znidarič, A., and Dempsey, A. T. (1999). "Comparison of two independently developed bridge weigh-in-motion systems." *Int. J. Heavy Veh. Syst.*, [6\(1–4\)](#), 147–161.

Peters, R. (1984). "Axway—A system to obtain vehicle axle weights." *Aust. Road Res.*, [12\(2\)](#), 10–18.

Shi, X., and Cai, C. (2009). "Simulation of dynamic effects of vehicles on pavement using a 3d interaction model." *J. Transp. Eng.*, [10.1061/\(ASCE\)TE.1943-5436.0000045](#), 736–744.

Wang, T.-L., and Liu, C. (2000). "Influence of heavy trucks on highway bridges." *Res. Rep. FL/DOT/RMC/6672-379*, Florida Dept. of Transportation, Tallahassee, FL.

WAVE. (2001). "Weighing-in-motion of axles and vehicles for europe (wave)." *Rep. of Work Package 1.2*, Laboratoire Central des Ponts et Chaussées, Paris.

Wu, J., and Chen, S. (2009). "Traffic flow simulation on bridge with cellular automaton technique." *Proc., Transportation Research Board*

88th Annual Meeting, Transportation Research Board, Washington DC.

Zhang, Y., Cai, C. S., Shi, X., and Wang, C. (2006). "Vehicle-induced dynamic performance of FRP versus concrete slab bridge." *J. Bridge Eng.*, [10.1061/\(ASCE\)1084-0702\(2006\)11:4\(410\)](https://doi.org/10.1061/(ASCE)1084-0702(2006)11:4(410)), 410–419.

Zhou, Y., and Chen, S. (2015). "Fully coupled driving safety analysis of moving traffic on long-span bridges subjected to crosswind." *J. Wind Eng. Ind. Aerodyn.*, *143*, 1–18.

Zhu, X. Q., and Law, S. S. (2000). "Identification of vehicle axle loads from bridge dynamic responses." *J. Sound Vib.*, *236*(4), 705–724.